PCCP

ROYAL SOCIETY OF CHEMISTRY

PAPER

View Article Online
View Journal | View Issue

Cite this: *Phys. Chem. Chem. Phys.*, 2025, **27**, 21022

Investigation of the structure–performance correlation in Y-series electron acceptors with different phenyl alkyl inner side chains toward high-efficiency organic solar cells

Jingyao Kong, Yufan Zhu, Bowen Li, Dan He * and Fuwen Zhao

Received 8th July 2025,
Accepted 4th September 2025

DOI: 10.1039/d5cp02606g

rsc.li/pccp

Y-Series non-fullerene acceptors (NFAs) make significant contributions to the booming efficiency of organic solar cells (OSCs). In particular, modifying inner side chains with phenyl groups affords an efficient and promising method to improve the efficiency and promote the large-area fabrication of OSCs. However, the relationship between the structure of the inner side chains and properties has rarely been investigated. In this work, three NFAs, Y6-PhC4, Y6-PhC6 and Y6-PhC8, are developed by introducing phenyl alkyl inner side chains with different lengths. It demonstrates that the length of the phenyl alkyl side chains has a negligible influence on the bandgap and energy levels of NFAs. However, the miscibility between NFAs and D18 declines along with the length of the phenyl alkyl inner side chains. Y6-PhC6 possesses the best crystallinity and D18:Y6-PhC6 blend films afford the finest topological morphology. Thus, the devices exhibit the tendency of first increasing and then decreasing in charge carrier dynamics, trap density and non-radiative recombination energy loss, which makes V_{OC}, J_{SC} and FF of OSCs show the same trend from D18:Y6-PhC4 and D18:Y6-PhC6 to D18:Y6-PhC8 pairs. Therefore, D18:Y6-PhC6 based devices achieve the highest power conversion efficiency (PCE) of 17.12%. Furthermore, D18:L8-BO:Y6-PhC6 based ternary OCSs are fabricated to afford an impressive PCE of 19.22%, benefiting from the superior properties of Y6-PhC6. This work manifests the importance of inner side chain engineering in regulating intrinsic properties and photovoltaic performance of Y-series NFAs.

Introduction

Organic solar cells (OSCs) have attracted considerable attention due to their distinct merits of ultra-flexible, light weight and low-cost solution processing.[1–3] The past three decades have witnessed the booming efficiency of OSCs, which benefits from the rapid development of non-fullerene acceptors (NFAs),[4–6] including A–D–A type (ITIC-series)[7–9] and A–DA′D–A type (Y-series).[10,11] Recently, the state-of-the-art Y-series NFAs have boosted the power conversion efficiencies (PCEs) of OSCs to surpass 20%, showing significant potential for industrialization.[12–15]

The chemical structure of Y-series NFAs consists of three parts: the donor unit, two electron-withdrawing end groups, and side chains which are attached to the β-position of the outermost thiophene (or selenophene) rings of the central core (*i.e.* outer side chains) and to inner pyrrole rings (*i.e.* inner side chains). Most reported Y-series molecules are evolved out of BZIC[16] or Y6,[10] *via* modifying donor units,[17] end groups[15] and side-chain engineering.[18–21] Among the strategies, side-chain engineering, mainly on outer side chains, is most widely employed, since manipulating outer side chains can efficiently improve the photovoltaic performance *via* regulating solubility, miscibility and molecular stacking.[22–24] In contrast to outer side-chain modification, adjusting inner side chains endows Y-series NFAs with distinctive properties, such as excellent non-halogenated solvent processing,[25] improved permittivity,[26,27] enhanced Marangoni flow,[28] and a self-regulation effect to modulate intermolecular packing.[29] For instance, Liu *et al.* designed a new NFA, Z9, by tethering four phenyl groups at the end of the Y6 inner side chains.[29] The phenyl groups induce intramolecular packing *via* the π–π stacking of phenyl-phenyl groups and improve intermolecular interaction, resulting in high crystallinity for reduced energy loss and enhanced open-circuit voltage (V_{OC}). Wu *et al.* further modified the phenyl end group of the inner side chains *via* introducing methyl, and obtained the NFA, L8-PhMe, which affords more orderly molecular packing to improve charge carrier mobilities and inhibit charge carrier recombination loss.[30] Therefore, modifying

State Key Laboratory of Powder Metallurgy, College of Chemistry and Chemical Engineering, Central South University, Changsha 410083, P. R. China. E-mail: hedancsu@csu.edu.cn

inner side chains with phenyl groups provides an effective and promising route to improve the efficiency and advance the large-area fabrication of OSCs. However, the relationship between phenyl inner side-chain structures and properties of NFAs has rarely been investigated.

In this work, we designed and synthesized three NFAs, Y6-PhC4, Y6-PhC6 and Y6-PhC8, with phenyl alkyl inner side chains having different lengths to study the structure–performance correlation in Y-series NFAs. Different from the common place, lengthening the phenyl alkyl inner side chains of the NFAs endows them with decreased miscibility with the classical polymer donor, D18. Among them, the D18:Y6-PhC6 blend film exhibits proper phase separation and the highest crystallinity, leading to the most efficient exciton dissociation and charge carrier transport. Moreover, D18:Y6-PhC6 based devices present the lowest trap density, and thus the highest mobility and weakest charge carrier recombination. Therefore, D18:Y6-PhC6 based OSCs afford the best PCE of 17.12%. Considering the superiority of Y6-PhC6, we further fabricated ternary OSCs based on D18:L8-BO:Y6-PhC6, which achieve a PCE as high as 19.22%. These findings highlight the importance of inner side-chain engineering in regulating the properties and photovoltaic performance of Y-series NFAs.

Results and discussion

The chemical structures and synthetic routes of Y6-PhC4, Y6-PhC6 and Y6-PhC8 are shown in Scheme S1 and Fig. 1a. The synthetic details are presented in the SI. The chemical structures of the intermediates and final products are confirmed by NMR and mass spectra (Fig. S1–S6). In addition, we successfully obtained the single crystal of Y6-PhC6 (Table S1). Y6-PhC6 molecules are packed in lamellar structures (Fig. S7), rather than forming classical 3D packing like Y6, which indicates that the chemical structure of the inner side chains plays an important role in the molecular aggregation of Y-series acceptors. The solution and thin-film absorption spectra of D18, Y6-PhC4, Y6-PhC6 and Y6-PhC8 were recorded on a UV-Vis spectrophotometer. In solution, the three NFAs show similar absorption with the maximum absorption peak at 731 nm (Fig. S8). From solution to thin-film states, all of them exhibit an obvious redshift with the maximum absorption peak at ~785 nm (Fig. 1b and Table S2). The absorption onsets of Y6-PhC4, Y6-PhC6 and Y6-PhC8 thin films are 880, 875 and 871 nm, respectively, corresponding to the optical bandgaps of 1.41 eV, 1.42 eV and 1.42 eV, respectively. It should be noted that, compared with Y6-PhC4 and Y6-PhC8, Y6-PhC6 exhibits a sharper absorption edge, which promises a reduced non-radiative recombination energy loss (ΔE_{nr}) for Y6-PhC6 based OSCs.[8,31] Moreover, the absorption of the Y6-PhC6 neat film demonstrates a larger intensity ratio between the A_{0-0} peak and A_{0-1} peak, which implies stronger crystallinity of Y6-PhC6 than Y6-PhC4 and Y6-PhC8 in neat films.[32] The energy levels of Y6-PhC4, Y6-PhC6 and Y6-PhC8 were deduced from the oxidation/reduction potentials (E_{ox}^{on}/E_{red}^{on}), which are estimated by cyclic voltammetry (Fig. 1c and Fig. S9). The highest occupied molecular orbital (HOMO) and lowest unoccupied molecular orbital (LUMO) energy levels of Y6-PhC4, Y6-PhC6 and Y6-PhC8 were calculated to be −5.64/−3.75, −5.65/−3.74 and −5.66/−3.74 eV, respectively, according to the empirical equations (Table S2). Thus, the length of the phenyl inner side chains has a negligible influence on the energy levels of NFAs. It should be noted that D18 was chosen as the electron donor in this work, because of its complementary absorption (Fig. 1b) and well-matched energy levels with Y6-PhC4, Y6-PhC6 and Y6-PhC8 (Fig. S10a and Table S2), which are helpful to obtain high short-circuit current density (J_{SC}) and V_{OC} in OSCs.

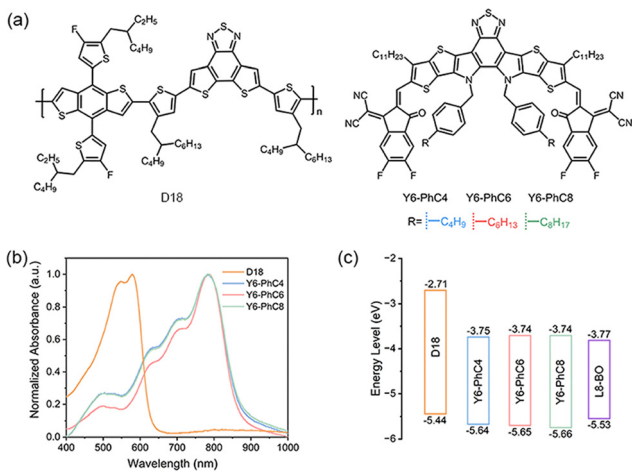

Fig. 1 (a) Chemical structures of D18 and NFAs. (b) UV-Vis absorption spectra of D18, Y6-PhC4, Y6-PhC6 and Y6-PhC8 neat films. (c) Energy level diagrams of D18, Y6-PhC4, Y6-PhC6, Y6-PhC8 and L8-BO.

Miscibility between the electron donor and acceptor governs the morphology of the active layer, which determines the photovoltaic performance of OSCs to some extent.[33,34] Thus, the miscibility between D18 and NFAs was firstly evaluated by determining the Flory–Huggins interaction parameter (χ) between them based on their surface free energy (γ).[35–37] The contact angles of water and glycerol on D18, Y6-PhC4, Y6-PhC6 and Y6-PhC8 thin films are 102.12°/91.51°, 94.02°/91.90°, 93.00°/91.49°, and 91.50°/87.03°, respectively (Fig. S11). According to Wu's model,[38] the γ values of D18, Y6-PhC4, Y6-PhC6 and Y6-PhC8 were calculated to be 20.60, 22.05, 22.63 and 24.05 mN m^{-1}, respectively (Table S3). Therefore, the χ_s values for the D18/Y6-PhC4, D18/Y6-PhC6 and D18/Y6-PhC8 pairs are 0.025 K, 0.048 K and 0.13 K, respectively, since the χ is directly proportional to $\left(\sqrt{\gamma_{D18}} - \sqrt{\gamma_{NFA}}\right)^2$.[39] This signifies that the miscibility between D18 and NFAs reduces along with the increased length of the phenyl inner side chains. This tendency is contrary to the most common place that the longer the side chains, the better miscibility between the donor and acceptor. The probable reason for this abnormal phenomenon is that phenyl inner side chains introduce a unique molecular packing mode *via* the phenyl-phenyl and phenyl-end group intermolecular interactions.[29]

To investigate the influence of the length of the phenyl alkyl inner side chain on photovoltaic performance, conventional

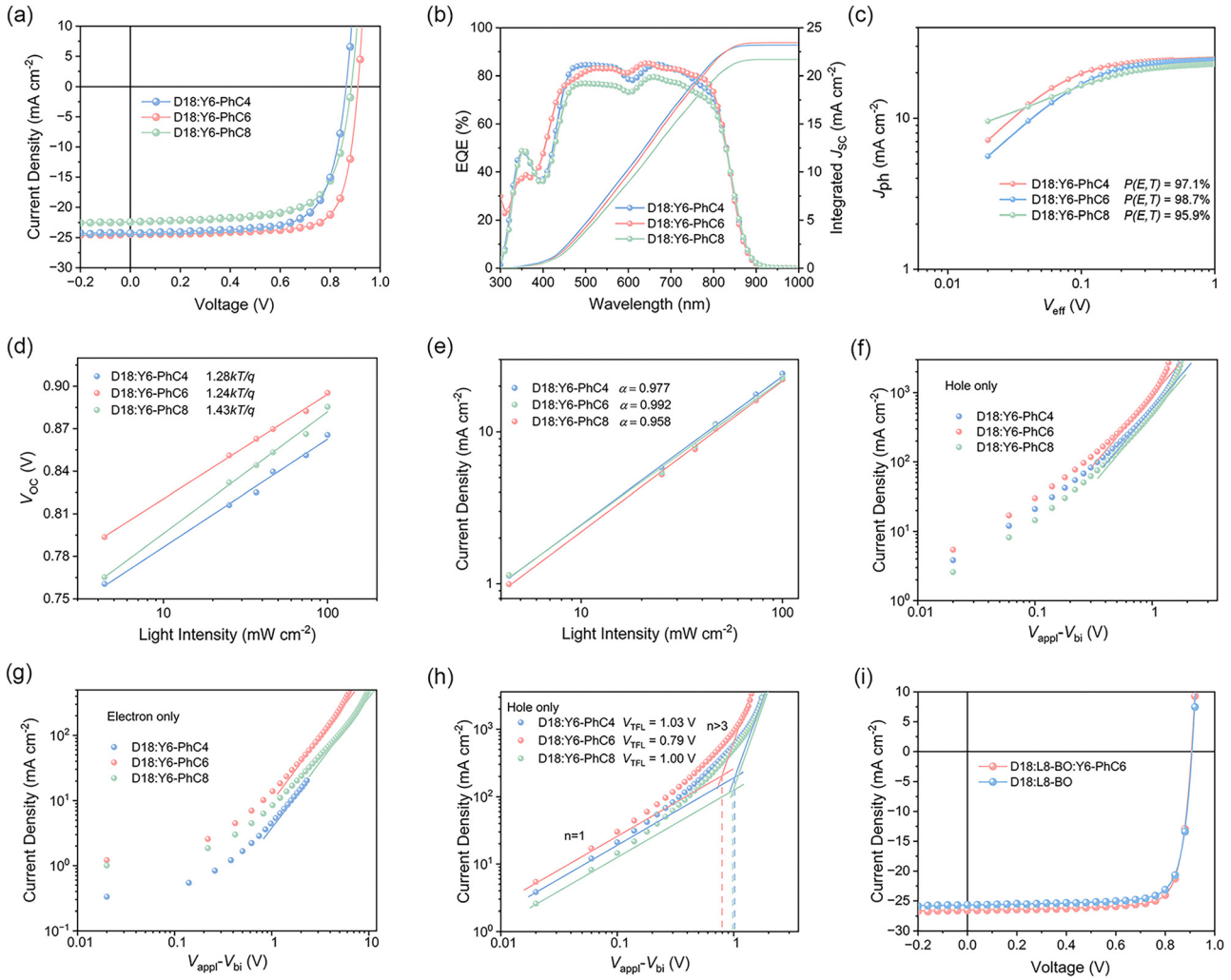

Fig. 2 (a) J–V curves and (b) EQE spectra of the D18:NFA-based OSCs. (c) Photocurrent density *versus* effective voltage curves of D18:NFA-based OSCs. (d) Dependence of V_{OC} on light intensity for D18:NFA-based OSCs. (e) Dependence of J_{SC} on light intensity for D18:NFA-based OSCs. (f) Typical current density-applied voltage semi-log plots for the hole-only devices based on the D18:NFA blend film (in the dark). (g) Typical current density-applied voltage semi-log plots for the electron-only devices based on D18:NFA blend film (in the dark). Measured data are shown as symbols while the solid lines are the best fits to the SCLC model. Mobilities were extracted from the fittings. (h) J–V characteristics of hole-only devices based on D18:NFA blend films (n represents the slope of the fitting lines). (i) J–V curves of D18:L8-BO and D18:L8-BO:Y6-PhC6-based OSCs.

devices with the configuration of ITO/PEDOT:PSS/D18:NFA/PDINN/Ag were fabricated. The J–V curves of the optimized devices are shown in Fig. 2a and the corresponding photovoltaic parameters are summarized in Table 1. The results demonstrate that V_{OC}, J_{SC} and fill factor (FF) show the tendency of first increasing and then decreasing from D18:Y6-PhC4 to D18:Y6-PhC6 to D18:Y6-PhC8-based OSCs. Thus, the D18:Y6-PhC6-based OSC achieves the highest PCE of 17.12% with the best V_{OC} of 0.912 V, J_{SC} of 24.49 mA cm^{-2} and FF of 76.73%. To further verify the J_{SC} from the J–V measurement, external quantum efficiencies (EQEs) of the optimized OSCs were determined. As shown in Fig. 2b, the calculated integration currents, obtained from the EQE curves, of D18:Y6-PhC4, D18:Y6-PhC6 and D18:Y6-PhC6-based devices are 23.20, 23.45

Table 1 Photovoltaic parameters of D18:NFA-based OSCs under AM 1.5G illumination at 100 mW cm^{-2}. The average values and standard deviations of 10 devices are shown in parentheses

	V_{oc} [V]	J_{SC} [mA cm^{-2}]	FF [%]	PCE [%]	J_{cal} [mA cm^{-2}]
D18:Y6-PhC4	0.864 (0.865 ± 0.003)	24.25 (23.90 ± 0.18)	71.65 (71.08 ± 0.39)	15.01 (14.70 ± 0.19)	23.20
D18:Y6-PhC6	0.912 (0.911 ± 0.004)	24.49 (23.76 ± 0.49)	76.73 (76.75 ± 0.84)	17.12 (16.63 ± 0.30)	23.45
D18:Y6-PhC8	0.885 (0.885 ± 0.005)	22.40 (22.29± 0.29)	70.05 (69.27 ± 0.76)	13.88 (13.66 ± 0.14)	21.70
D18:L8-BO	0.908 (0.910 ± 0.001)	25.68 (25.14 ± 0.21)	79.31 (79.78 ± 0.35)	18.50 (18.24 ± 0.14)	24.75
D18:L8-BO:Y6-PhC6	0.906 (0.909 ± 0.003)	26.53 (26.13 ± 0.38)	79.94 (79.90 ± 0.62)	19.22 (18.97 ± 0.17)	25.22

and 21.70 mA cm^{-2}, respectively, which all agree well with the values from their *J–V* curves (<5% mismatch).

To illustrate the structure–performance correlation in NFAs with phenyl alkyl inner side chains, the energy loss (ΔE) and charge carrier dynamics were analyzed. The E_gs for D18:Y6-PhC4, D18:Y6-PhC6 and D18:Y6-PhC8-based devices, which are extracted from the EQE spectra of the devices, are 1.470, 1.477 and 1.468 eV, respectively. According to $\Delta E = E_g - eV_{OC}$, the ΔEs for D18:Y6-PhC4, D18:Y6-PhC6 and D18:Y6-PhC8 based devices are 0.606, 0.565 and 0.583 eV, respectively. The lowest energy loss and thus highest V_{OC} for D18:Y6-PhC6 is related to the reduced non-radiative recombination energy loss, which is indicated by the sharp absorption onset of Y6-PhC6. The exciton dissociation and charge carrier recombination in D18:Y6-PhC4, D18:Y6-PhC6 and D18:Y6-PhC8-based devices were measured to study the influence of inner side chain length on charge carrier dynamics. The photocurrent density (J_{ph}) *versus* effective voltage (V_{eff}) was determined to evaluate the exciton dissociation probability $P(E,T)$ in OSCs.[40,41] $J_{ph} = J_L - J_D$, where J_L and J_D represent the current density under the illumination intensity and in the dark, respectively, while $V_{eff} = V_0 - V_a$, where V_0 is the voltage when J_{ph} is zero and V_a is the applied bias.[42] In addition, J_{sat} delegates the J_{ph} under a high V_{eff} (V_{eff} = 2 V is used in our work), where all photon-generated excitons are assumed to be dissociated into free charge carriers and then extracted by electrodes. As shown in Fig. 2c, the J_{sat}s of the D18:Y6-PhC4, D18:Y6-PhC6 and D18:Y6-PhC8-based devices are 24.98, 24.81 and 23.36 mA cm^{-2}, respectively. Under J_{SC} conditions, the $P(E,T) = J_{ph}/J_{sat}$ of the D18:Y6-PhC4, D18:Y6-PhC6 and D18:Y6-PhC8-based devices were calculated to be 97.1%, 98.7% and 95.9%, respectively, indicating the most efficient exciton dissociation in the D18:Y6-PhC6-based device.[43] The charge carrier recombination in the D18:Y6-PhC4, D18:Y6-PhC6 and D18:Y6-PhC8-based devices was determined *via* measuring the dependence of V_{OC} and J_{SC} on the incident light intensity (P_{light}). V_{OC} was plotted against $\ln[P_{light}]$ to evaluate the monomolecular recombination in the devices.[44] As shown in Fig. 2d, the slopes of the D18:Y6-PhC4, D18:Y6-PhC6 and D18:Y6-PhC8-based devices are $1.28kT/q$, $1.24kT/q$ and $1.43kT/q$, respectively, where T is the Kelvin temperature, k the Boltzmann constant, and q the elementary charge. The smallest slope for the D18:Y6-PhC6 based device among them indicates the weakest monomolecular recombination. The J_{SC}s of the D18:Y6-PhC4, D18:Y6-PhC6 and D18:Y6-PhC8-based devices under different P_{light} were also fitted to the power-law equation: $J_{SC} \propto [P_{light}]^{\alpha}$ (Fig. 2e).[45] The α values of the D18:Y6-PhC4, D18:Y6-PhC6 and D18:Y6-PhC8-based devices are 0.977, 0.992 and 0.958, respectively. That is, the D18:Y6-PhC6-based device affords the weakest bimolecular recombination, since its α value is closest to 1.[46]

The charge carrier mobility was measured by space-charge-limiting current (SCLC).[47] As shown in Fig. 2f and g, the hole mobilities (μ_hs) for the D18:Y6-PhC4, D18:Y6-PhC6 and D18:Y6-PhC8-based devices are 3.77×10^{-3}, 5.28×10^{-3} and 2.97×10^{-3} cm^{-2} V^{-1} s^{-1}, respectively, while the electron mobilities (μ_es) for them are 1.96×10^{-5}, 4.26×10^{-5} and 1.77×10^{-5} cm^{-2} V^{-1} s^{-1}, respectively (Table S4). The highest μ_h and μ_e for the D18:Y6-PhC6-based devices would benefit charge carrier transport for enhanced J_{SC} and FF. In short, for the devices based on D18:Y6-PhC4, D18:Y6-PhC6 and D18:Y6-PhC8, $P(E,T)$, monomolecular and bimolecular recombination, and charge carrier mobilities all show the evolution of first increasing and then decreasing, which is highly consistent with the tendency of J_{SC} and FF in OSCs. Among them, the D18:Y6-PhC6-based devices have the most efficient exciton dissociation, weakest monomolecular and bimolecular recombination, and highest charge carrier mobility, thus contributing to the highest J_{SC} and FF in OSCs.

The total trap density (N_t) in the device was also measured by the SCLC method, according to the following equation:[48]

$$N_t = \frac{2\varepsilon_0 \varepsilon V_{TFL}}{qL^2}$$

where ε_0 is the permittivity of vacuum, ε the relative dielectric constant of the active layer materials (typically, it is 3.0 for organic photovoltaic materials.), V_{TFL} the trap-filled limit voltage, and L the thickness of the active layer. As shown in Fig. 2h, the V_{TFL}s were determined to be 1.03, 0.79 and 1.00 V, respectively. Therefore, the N_ts in the D18:Y6-PhC4, D18:Y6-PhC6 and D18:Y6-PhC8-based devices were calculated to be 2.19×10^{16}, 1.82×10^{16} and 2.31×10^{16} cm^{-3}, respectively. The D18:Y6-PhC6 based device exhibits the lowest trap density, which is related to the strong crystallinity of Y6-PhC6 and affords the weakest monomolecular recombination.[49] Furthermore, the ΔE_{nr} of the devices was determined by using electroluminescence quantum efficiency (EQE_{EL}) measurements.50 As shown in Fig. S12, the D18:Y6-PhC6 based device presents a higher EQE_{EL} of 7.89×10^{-5} than the D18:Y6-PhC4 (5.79×10^{-5}) one. According to the equation: $\Delta E_{nr} = -kT\ln(EQE_{EL})$, the D18:Y6-PhC6 based device affords a smaller ΔE_{nr} of 0.243 eV, compared to 0.251 eV for the D18:Y6-PhC4 pair, which contributes to the reduced ΔE in OSCs. Note that the undetermined EQE_{EL} for the D18:Y6-PhC8 based device may be ascribed to a too small value out of the detection limit of the apparatus.

To clarify the relationship between charge carrier dynamics in PM6:NFA-based devices and material properties, the morphology of PM6:NFA blend films was further investigated by using atomic force microscopy (AFM). As shown in the height images (Fig. 3a–c), the root-mean-square roughness values of the D18:Y6-PhC4, D18:Y6-PhC6 and D18:Y6-PhC8 blend films are 1.11, 3.86, and 7.35 nm, respectively. To further compare the details of phase separation, line profiles across the phase images of the blend films (Fig. 3d–f) are shown in Fig. 3g–i. The full-width at half-maximum (FWHM) of the peaks is used to estimate the fibril diameter. The D18:Y6-PhC4 blend film exhibits fine nanofibers with FWHM of 12.49 nm, which is beneficial to exciton dissociation, and thus a $P(E,T)$ as high as 97.1% is realized in D18:Y6-PhC4-based OSCs. However, too small domain size would aggravate bimolecular recombination to some extent. In the D18:Y6-PhC6 blend film, nanofibers with

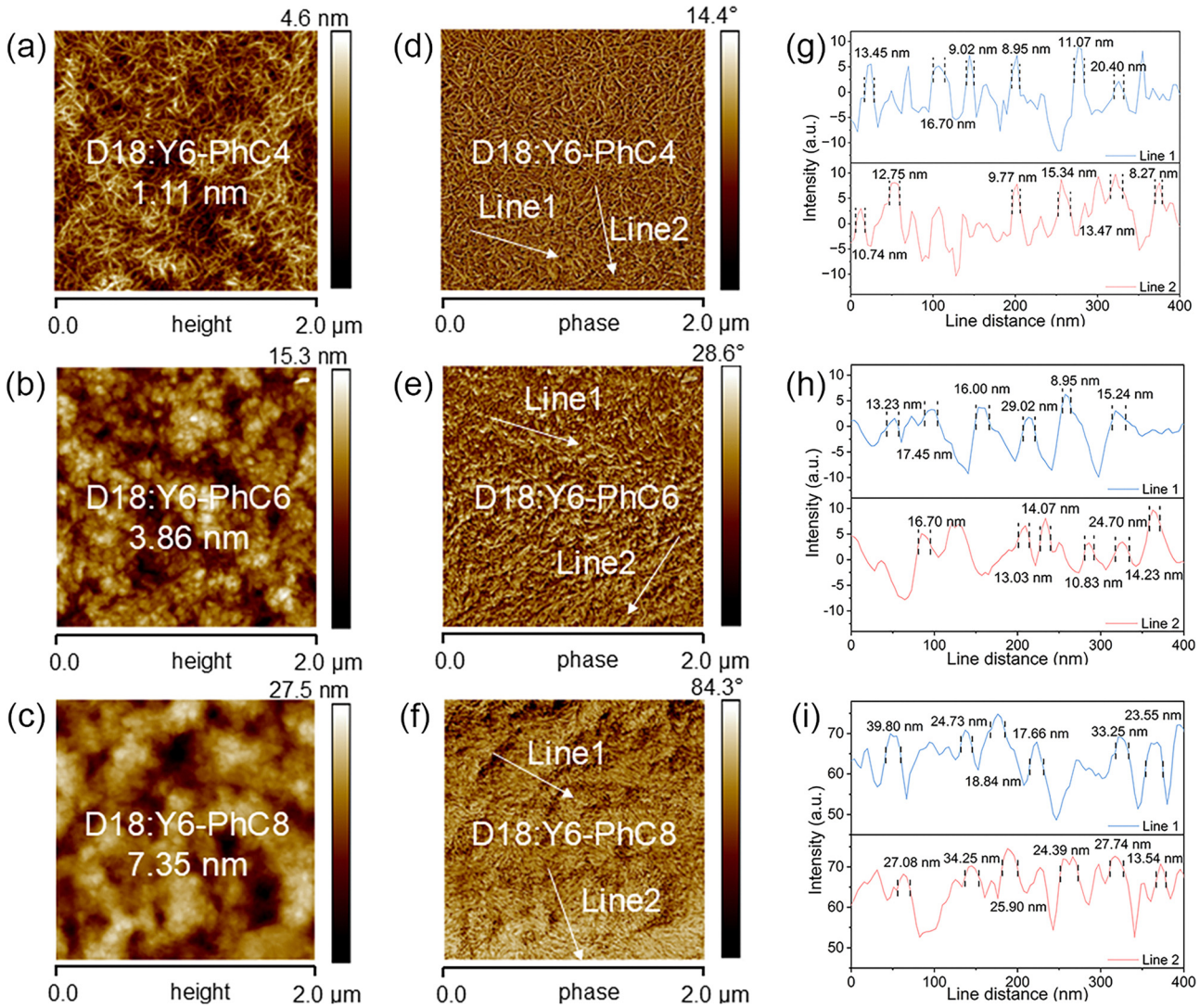

Fig. 3 AFM height images of (a) D18:Y6-PhC4, (b) D18:Y6-PhC6 and (c) D18:Y6-PhC8 blend films. AFM phase images of (d) D18:Y6-PhC4, (e) D18:Y6-PhC6 and (f) D18:Y6-PhC8 blend films. Line profiles along the location of the solid white lines in the panels to obtain the grain sizes in (g) D18:Y6-PhC4, (h) D18:Y6-PhC6 and (i) D18:Y6-PhC8 blend films. The nano-grain size in each case was specifically calculated from the FWHM (the distance between two adjacent dashed lines in the graphs).

FWHM of 16.12 nm and proper phase separation were observed. Thus, the most efficient exciton dissociation and charge carrier transport are acquired, contributing to the highest J_{SC} and FF in D18:Y6-PhC6-based devices. In the D18:Y6-PhC8 blend film, nanofibers with FWHM of 25.89 nm are observed. This implies excessive phase separation, which leads to inferior $P(E,T)$ and severe charge carrier recombination. Thus, the D18:Y6-PhC8 based device suffers the highest leakage current (Fig. S13).

Considering the superiority of Y6-PhC6, including high crystallinity, low trap density and proper miscibility with donors, *etc.*, we employed Y6-PhC6 as the third component to improve the photovoltaic performance of D18:L8-BO (note that L8-BO has similar energy levels with Y6-PhC6 (Fig. 1c)), which is the most representative donor and acceptor pair currently. As shown in Fig. 2i, the binary OSCs based on D18:L8-BO deliver a PCE of 18.50%, which is comparable with the value in the reported literature.[51] The addition of Y6-PhC6 improves the J_{SC} from 25.68 to 26.53 mA cm^{-2} and the FF from 79.31% to 79.94%. As a result, the D18:L8-BO:Y6-PhC6 (1 : 1 : 0.1)-based ternary OSCs achieve an impressive PCE as high as 19.22%. The EQE spectra of the D18:L8-BO and D18:L8-BO:Y6-PhC6 based devices were also determined to verify the J_{SC} (Fig. S14). The calculated integration currents, obtained from the EQE curves for D18:L8-BO and D18:L8-BO:Y6-PhC6 based OSCs are 24.75 and 25.22 mA cm^{-2}, respectively, which are highly consistent with the J_{SC}s from their J–V curves (<5% mismatch).

Conclusions

In this work, the structure–performance correlation in Y-series NFAs with phenyl alkyl inner side chains was systematically

investigated *via* developing three new NFAs, Y6-PhC4, Y6-PhC6 and Y6-PhC8 with a different length of the phenyl alkyl inner chains. As the phenyl inner side chains extend, the miscibility between them and D18 reduces. Thus, the domain size increases gradually from D18:Y6-PhC4 to D18:Y6-PhC6 to D18:Y6-PhC8. The highest crystallinity and moderate miscibility of Y6-PhC6 make the D18:Y6-PhC6 blend film possess the finest phase separation with FWHM of 16.12 nm and a long nanofiber structure, thus benefiting exciton dissociation and charge carrier transport. In addition, D18:Y6-PhC6 based OSCs exhibit the lowest trap density and thus the highest mobility and weakest charge carrier recombination. Therefore, D18:Y6-PhC6 based OSCs afford the highest PCE of 17.12% with enhanced V_{OC}, J_{SC} and FF. Furthermore, after introducing Y6-PhC6 into the D18:L8-BO system, an impressive PCE as high as 19.22% was realized. This work demonstrates that it is important to regulate the length of the phenyl alkyl inner side chains, which would endow NFAs with special characters. Furthermore, the research on the effects of phenyl alkyl inner side chains on intermolecular and intramolecular interactions is ongoing.

Author contributions

D. H. and F. Z. developed the conceptualization. Y. Z. and B. L. synthesized the materials and measured their photoelectrical properties. J. K. conducted device fabrication and characterization. The initial draft of the manuscript was written and revised by D. H. and F. Z. All authors have read and agreed to the published version of the manuscript.

Conflicts of interest

The authors declare no conflict of interest.

Data availability

The data supporting this article have been included as part of the SI. See DOI: **https://doi.org/10.1039/d5cp02606g**.

CCDC 2476416 contains the supplementary crystallographic data for this paper.[52]

Acknowledgements

The authors thank the National Natural Science Foundation of China (Grant No. 52372056, 52232003) and the Science and Technology Innovation Program of Hunan Province (Grant No. 2023RC3044) for financial support.

Notes and references

1 D. Li, N. Deng, Y. Fu, C. Guo, B. Zhou, L. Wang, J. Zhou, D. Liu, W. Li, K. Wang, Y. Sun and T. Wang, Fibrillization of Non-Fullerene Acceptors Enables 19% Efficiency Pseudo-Bulk Heterojunction Organic Solar Cells, *Adv. Mater.*, 2023, **35**, 2208211.

2 T. Dai, Y. Meng, Z. Wang, J. Lu, Z. Zheng, M. Du, Q. Guo and E. Zhou, Modulation of Molecular Quadrupole Moments by Phenyl Side-Chain Fluorination for High-Voltage and High-Performance Organic Solar Cells, *J. Am. Chem. Soc.*, 2025, **147**, 4631–4642.

3 F. Zhao, H. Zhang, R. Zhang, J. Yuan, D. He, Y. Zou and F. Gao, Emerging Approaches in Enhancing the Efficiency and Stability in Non-Fullerene Organic Solar Cells, *Adv. Energy Mater.*, 2020, **10**, 2002746.

4 X. Li, X. Kong, G. Sun and Y. Li, Organic Small Molecule Acceptor Materials for Organic Solar Cells, *eScience*, 2023, **3**, 100171.

5 C. Yan, S. Barlow, Z. Wang, H. Yan, A. K.-Y. Jen, S. R. Marder and X. Zhan, Non-Fullerene Acceptors for Organic Solar Cells, *Nat. Rev. Mater.*, 2018, **3**, 18003.

6 J. Wang, Y. Xie, K. Chen, H. Wu, J. M. Hodgkiss and X. Zhan, Physical Insights into Non-Fullerene Organic Photovoltaics, *Nat. Rev. Phys.*, 2024, **6**, 365–381.

7 Y. Lin, J. Wang, Z.-G. Zhang, H. Bai, Y. Li, D. Zhu and X. Zhan, An Electron Acceptor Challenging Fullerenes for Efficient Polymer Solar Cells, *Adv. Mater.*, 2015, **27**, 1170–1174.

8 J. Zhou, D. He, Y. Li, F. Huang, J. Zhang, C. Zhang, Y. Yuan, Y. Lin, C. Wang and F. Zhao, Reducing Trap Density in Organic Solar Cells via Extending the Fused Ring Donor Unit of an A-D-A-Type Nonfullerene Acceptor for over 17% Efficiency, *Adv. Mater.*, 2023, **35**, 2207336.

9 F. Zhao, S. Dai, Y. Wu, Q. Zhang, J. Wang, L. Jiang, Q. Ling, Z. Wei, W. Ma, W. You, C. Wang and X. Zhan, Single-Junction Binary-Blend Nonfullerene Polymer Solar Cells with 12.1% Efficiency, *Adv. Mater.*, 2017, **29**, 1700144.

10 J. Yuan, Y. Zhang, L. Zhou, G. Zhang, H.-L. Yip, T.-K. Lau, X. Lu, C. Zhu, H. Peng, P. A. Johnson, M. Leclerc, Y. Cao, J. Ulanski, Y. Li and Y. Zou, Single-Junction Organic Solar Cell with over 15% Efficiency Using Fused-Ring Acceptor with Electron-Deficient Core, *Joule*, 2019, **3**, 1140–1151.

11 J. Yuan, H. Zhang, R. Zhang, Y. Wang, J. Hou, M. Leclerc, X. Zhan, F. Huang, F. Gao, Y. Zou and Y. Li, Reducing Voltage Losses in the A-DA'D-A Acceptor-Based Organic Solar Cells, *Chem*, 2020, **6**, 2147–2161.

12 J. Wang, P. Xue, Y. Jiang, Y. Huo and X. Zhan, The Principles, Design and Applications of Fused-Ring Electron Acceptors, *Nat. Rev. Chem.*, 2022, **6**, 614–634.

13 Y. Jiang, F. Liu and X. Zhu, Single-Junction Organic Solar Cells with a Power Conversion Efficiency of More than 20%, *Nat. Energy*, 2024, **9**, 930–931.

14 C. Chen, L. Wang, W. Xia, K. Qiu, C. Guo, Z. Gan, J. Zhou, Y. Sun, D. Liu, W. Li and T. Wang, Molecular Interaction Induced Dual Fibrils Towards Organic Solar Cells with Certified Efficiency over 20%, *Nat. Commun.*, 2024, **15**, 6865.

15 Y. Jiang, S. Sun, R. Xu, F. Liu, X. Miao, G. Ran, K. Liu, Y. Yi, W. Zhang and X. Zhu, Non-Fullerene Acceptor with Asymmetric Structure and Phenyl-Substituted Alkyl Side Chain

for 20.2% Efficiency Organic Solar Cells, *Nat. Energy*, 2024, **9**, 975–986.
16 L. Feng, J. Yuan, Z. Zhang, H. Peng, Z.-G. Zhang, S. Xu, Y. Liu, Y. Li and Y. Zou, Thieno[3,2-b]pyrrolo-Fused Pentacyclic Benzotriazole-Based Acceptor for Efficient Organic Photovoltaics, *ACS Appl. Mater. Interfaces*, 2017, **9**, 31985–31992.
17 K. Liu, Y. Jiang, G. Ran, F. Liu, W. Zhang and X. Zhu, 19.7% Efficiency Binary Organic Solar Cells Achieved by Selective Core Fluorination of Nonfullerene Electron Acceptors, *Joule*, 2024, **8**, 835–851.
18 C. Han, B. Cheng, Z. Fu, H. Wang, S. Ji, J. Wu, S. Cheng, X. Xia, H. Yin and X. Du, Vinyl-Functionalized Linear Alkyl Chains in Nonfullerene Acceptors Enable 19.2% Efficiency and Stable As-Cast Organic Solar Cells, *Angew. Chem., Int. Ed.*, 2025, **137**, e202501592.
19 Y. Chen, F. Bai, Z. Peng, L. Zhu, J. Zhang, X. Zou, Y. Qin, H. K. Kim, J. Yuan, L.-K. Ma, J. Zhang, H. Yu, P. C. Y. Chow, F. Huang, Y. Zou, H. Ade, F. Liu and H. Yan, Asymmetric Alkoxy and Alkyl Substitution on Nonfullerene Acceptors Enabling High-Performance Organic Solar Cells, *Adv. Energy Mater.*, 2021, **11**, 2003141.
20 Y. Chen, H. Meng, L. Ding, J. Tang, J. Yi, J. Zhang, Z. Wang, R. Ma, Z. Li, L. Lyu, X. Xu, Q. Peng, H. Yan and H. Hu, Asymmetric Non-Fullerene Acceptors with Branched Alkyl-Chains for Efficient Organic Solar Cells with High Open-Circuit Voltage, *Chem. Mater.*, 2022, **34**, 10144–10152.
21 C. Xiao, X. Wang, T. Zhong, R. Zhou, X. Zheng, Y. Liu, T. Hu, Y. Luo, F. Sun, B. Xiao, Z. Liu, C. Yang and R. Yang, Hybrid Cycloalkyl-Alkyl Chain-Based Symmetric/Asymmetric Acceptors with Optimized Crystal Packing and Interfacial Exciton Properties for Efficient Organic Solar Cells, *Adv. Sci.*, 2023, **10**, 2206580.
22 W. Liu, R. Zhang, Q. Wei, C. Zhu, J. Yuan, F. Gao and Y. Zou, Manipulating Molecular Aggregation and Crystalline Behavior of A-DA'D-A Type Acceptors by Side Chain Engineering in Organic Solar Cells, *Aggregate*, 2022, **3**, e183.
23 S. Dong, T. Jia, K. Zhang, J. Jing and F. Huang, Single-Component Non-halogen Solvent-Processed High-Performance Organic Solar Cell Module with Efficiency over 14%, *Joule*, 2020, **4**, 2004–2016.
24 L. Tian, C. Liu and F. Huang, Recent Progress in Side Chain Engineering of Y-series Non-Fullerene Molecule and Polymer Acceptors, *Sci. China: Chem.*, 2024, **67**, 788–805.
25 X. Wu, X. Jiang, X. Li, J. Zhang, K. Ding, H. Zhuo, J. Guo, J. Li, L. Meng, H. Ade and Y. Li, Introducing a Phenyl End Group in the Inner Side Chains of A-DA'D-A Acceptors Enables High-Efficiency Organic Solar Cells Processed with Nonhalogenated Solvent, *Adv. Mater.*, 2023, **35**, 2302946.
26 T. Li, K. Wang, G. Cai, Y. Li, H. Liu, Y. Jia, Z. Zhang, X. Lu, Y. Yang and Y. Lin, Asymmetric Glycolated Substitution for Enhanced Permittivity and Ecocompatibility of High-Performance Photovoltaic Electron Acceptor, *JACS Au*, 2021, **1**, 1733–1742.
27 J. Dong, Y. Li, C. Liao, X. Xu, L. Yu, R. Li and Q. Peng, Dielectric Constant Engineering of Nonfullerene Acceptors Enables a Record Fill Factor of 83.58% and a High Efficiency of 20.80% in Organic Solar Cells, *Energy Environ. Sci.*, 2025, **18**, 4982–4995.
28 G. Park, Y. Cho, S. Jeong, J. Park, S.-J. Yoon and C. Yang, Enhancing the Marangoni Flow by Inner Side Chain Engineering in Nonfullerene Acceptors for Reproducible Blade Coating-Processed Organic Solar Cell Manufacturing, *J. Mater. Chem. A*, 2023, **11**, 12185–12193.
29 F. Liu, Y. Jiang, R. Xu, W. Su, S. Wang, Y. Zhang, K. Liu, S. Xu, W. Zhang, Y. Yi, W. Ma and X. Zhu, Nonfullerene Acceptor Featuring Unique Self-Regulation Effect for Organic Solar Cells with 19% Efficiency, *Angew. Chem., Int. Ed.*, 2024, **63**, e202313791.
30 X. Wu, Y. Gong, X. Li, S. Qin, H. He, Z. Chen, T. Liang, C. Wang, D. Deng, Z. Bi, W. Ma, L. Meng and Y. Li, Inner Side Chain Modification of Small Molecule Acceptors Enables Lower Energy Loss and High Efficiency of Organic Solar Cells Processed with Non-Halogenated Solvents, *Angew. Chem., Int. Ed.*, 2025, **64**, e202416016.
31 Z. Zhang, Y. Li, G. Cai, Y. Zhang, X. Lu and Y. Lin, Selenium Heterocyclic Electron Acceptor with Small Urbach Energy for As-Cast High-Performance Organic Solar Cells, *J. Am. Chem. Soc.*, 2020, **142**, 18741–18745.
32 Y. Bai, K. Wang, X. Wu, D. He, X. Li, J. Zhang, Y. Li and F. Zhao, Prolonging Charge Carrier Lifetime via Reinforcing Molecular Stacking for High-Efficiency Organic Solar Cells, *J. Cent South Univ.*, 2024, **31**, 4307–4318.
33 F. Zhao, C. Wang and X. Zhan, Morphology Control in Organic Solar Cells, *Adv. Energy Mater.*, 2018, **8**, 1703147.
34 Z. Han, K. Wang, Y. Chai, R. Zhang, J. Zhang, D. He, C. Wang and F. Zhao, Regulating the Miscibility of Donors/Acceptors to Manipulate the Morphology and Reduce Non-Radiative Recombination Energy Loss Enables Efficient Organic Solar Cells, *J. Mater. Chem. C*, 2024, **12**, 3873–3880.
35 K.-H. Kim, H. Kang, H. J. Kim, P. S. Kim, S. C. Yoon and B. J. Kim, Effects of Solubilizing Group Modification in Fullerene Bis-Adducts on Normal and Inverted Type Polymer Solar Cells, *Chem. Mater.*, 2012, **24**, 2373–2381.
36 F. Zhao, D. He, C. Zou, Y. Li, K. Wang, J. Zhang, S. Yang, Y. Tu, C. Wang and Y. Lin, Fullerene-Liquid-Crystal-Induced Micrometer-Scale Charge-Carrier Diffusion in Organic Bulk Heterojunction, *Adv. Mater.*, 2023, **35**, 2210463.
37 Z. Lin, Q. Ai, X. Wu, Y. Zhu, K. Wang, X. Li, D. He, Y. Zhang, J. Zhang, Y. Li and F. Zhao, As-Cast Organic Solar Cells with 19.44% Efficiency Enabled by Introducing Functional Fullerene Derivative to Facilitate Charge Carrier Generation and Transport, *Sci. China: Chem.*, 2025, **68**, 1991–1997.
38 J. Comyn, Contact Angles and Adhesive Bonding, *Int. J. Adhes. Adhes.*, 1992, **12**, 145–149.
39 S. Nilsson, A. Bernasik, A. Budkowski and E. Moons, Morphology and Phase Segregation of Spin-Casted Films of Polyfluorene/PCBM Blends, *Macromolecules*, 2007, **40**, 8291–8301.
40 Y. Zhu, D. He, C. Wang, X. Han, Z. Liu, K. Wang, J. Zhang, X. Shen, J. Li, Y. Lin, C. Wang, Y. He and F. Zhao,

Suppressing Exciton-Vibration Coupling to Prolong Exciton Lifetime of Nonfullerene Acceptors Enables High-Efficiency Organic Solar Cells, *Angew. Chem. Int. Ed.*, 2024, **63**, e202316227.

41 L. Lu, T. Xu, W. Chen, E. S. Landry and L. Yu, Ternary Blend Polymer Solar Cells with Enhanced Power Conversion Efficiency, *Nat. Photonics*, 2014, **8**, 716–722.

42 K. Wang, F. Zhao, Y. Zhu, Y. He, Z. Liu, X. Han, Q. Ai, X. Shen, B. Li, J. Zhang, Y. Lin, C. Wang and D. He, Prolonging the Exciton Diffusion Length by Manipulating Molecular Stacking Enables Pseudo-Planar Heterojunction Organic Solar Cells to Achieve over 19% Efficiency, *J. Mater. Chem. A*, 2024, **12**, 12208–12215.

43 Q. Ai, Z. Lin, X. Wu, Y. Zhu, K. Wang, X. Li, J. Zhang, D. He, Y. Li and F. Zhao, Ternary Polythiophene Enables over 17% Efficiency Organic Solar Cells, *J. Mater. Chem. A*, 2024, **12**, 10984–10990.

44 W. L. Leong, S. R. Cowan and A. J. Heeger, Differential Resistance Analysis of Charge Carrier Losses in Organic Bulk Heterojunction Solar Cells: Observing the Transition from Bimolecular to Trap-Assisted Recombination and Quantifying the Order of Recombination, *Adv. Energy Mater.*, 2011, **1**, 517–522.

45 S. R. Cowan, A. Roy and A. J. Heeger, Recombination in Polymer-Fullerene Bulk Heterojunction Solar Cells, *Phys. Rev. B: Condens. Matter Mater. Phys.*, 2010, **82**, 245207.

46 D. He, J. Zhou, Y. Zhu, Y. Li, K. Wang, J. Li, J. Zhang, B. Li, Y. Lin, Y. He, C. Wang and F. Zhao, Manipulating Vertical Phase Separation Enables Pseudoplanar Heterojunction Organic Solar Cells over 19% Efficiency via Ternary Polymerization, *Adv. Mater.*, 2024, **36**, 2308909.

47 V. M. L. Corre, E. A. Duijnstee, O. E. Tambouli, J. M. Ball, H. J. Snaith, J. Lim and L. J. A. Koster, Revealing Charge Carrier Mobility and Defect Densities in Metal Halide Perovskites via Space-Charge-Limited Current Measurements, *ACS Energy Lett.*, 2021, **6**, 1087–1094.

48 K. Wang, D. He, L. Jiang, C. Wang and F. Zhao, Investigation of Isomerization Effects on the Photovoltaic Performance of Fused-Ring Electron Acceptors via Side-Chain Position Manipulation, *J. Mater. Chem. C*, 2023, **11**, 2063–2068.

49 D. He, Y. Li, F. Zhao and Y. Lin, Trap Suppression in Ordered Organic Photovoltaic Heterojunctions, *Chem. Commun.*, 2024, **60**, 364–373.

50 D. He, F. Zhao, C. Wang and Y. Lin, Non-Radiative Recombination Energy Losses in Non-Fullerene Organic Solar Cells, *Adv. Funct. Mater.*, 2022, **32**, 2111855.

51 L. Zhu, M. Zhang, J. Xu, C. Li, J. Yan, G. Zhou, W. Zhong, T. Hao, J. Song, X. Xue, Z. Zhou, H. Zhu, C.-C. Chen, R. C. I. MacKenzie, Y. Zou, J. Nelson, Y. Zhang, Y. Sun and F. Liu, Single-Junction Organic Solar Cells with over 19% Efficiency Enabled by a Refined Double-Fibril Network Morphology, *Nat. Mater.*, 2022, **21**, 656–663.

52 J. Kong, Y. Zhu, B. Li, D. He and F. Zhao, CCDC 2476416: Experimental Crystal Structure Determination, 2025, DOI: **10.5517/sccdc.csd.cc2p3yvm**.